

Micromechanical model of a surrogate for collagenous soft tissues: development, validation and analysis of mesoscale size effects

Shawn P. Reese · Benjamin J. Ellis · Jeffrey A. Weiss

Received: 28 June 2012 / Accepted: 25 January 2013
© Springer-Verlag Berlin Heidelberg 2013

Abstract Aligned, collagenous tissues such as tendons and ligaments are composed primarily of water and type I collagen, organized hierarchically into nanoscale fibrils, microscale fibers and mesoscale fascicles. Force transfer across scales is complex and poorly understood. Since innervation, the vasculature, damage mechanisms and mechanotransduction occur at the microscale and mesoscale, understanding multiscale interactions is of high importance. This study used a physical model in combination with a computational model to isolate and examine the mechanisms of force transfer between scales. A collagen-based surrogate served as the physical model. The surrogate consisted of extruded collagen fibers embedded within a collagen gel matrix. A micromechanical finite element model of the surrogate was validated using tensile test data that were recorded using a custom tensile testing device mounted on a confocal microscope. Results demonstrated that the experimentally measured macroscale strain was not representative of the microscale strain, which was highly inhomogeneous. The micromechanical model, in combination with a macroscopic continuum model, revealed that the

microscale inhomogeneity resulted from size effects in the presence of a constrained boundary. A sensitivity study indicated that significant scale effects would be present over a range of physiologically relevant inter-fiber spacing values and matrix material properties. The results indicate that the traditional continuum assumption is not valid for describing the macroscale behavior of the surrogate and that boundary-induced size effects are present.

Keywords Collagen · Soft tissue · Ligament · Tendon · Composites · Biomechanics · Finite element method

1 Introduction

Collagenous soft tissues such as ligaments, tendon, skin, cornea, cartilage and intervertebral disk are composite materials, composed primarily of collagen, with lesser amounts of noncollagenous extracellular matrix (ECM) components and water. From an engineering perspective, these connective tissues are astounding structures. These materials exhibit a multiscale, hierarchical organization of collagen, from the nanometer to the millimeter, and their macroscopic material properties are derived from a complex, multiscale organization of collagen and other ECM proteins. At the nanoscale, tropocollagen monomers self-assemble to form fibrils (50–200 nm diameter), which display a characteristic d-banding (Ottani et al. 2001, 2002; Venturoni et al. 2003; Kannus 2000). Fibrils are spaced regularly within healthy tissue and predominantly aligned in parallel (Vidal 2003; Starborg et al. 2009; Birk et al. 1997). At the microscale, fibrils are assembled into fibers (20–50 μm diameter) (Jarvinen et al. 2004; Danylchuk et al. 1978). Fibroblasts (tenocytes in tendon) are located in the inter-fiber space. The characteristic crimp pattern is visible at the fiber level, with a period of 50–200 μm

Electronic supplementary material The online version of this article (doi:10.1007/s10237-013-0475-2) contains supplementary material, which is available to authorized users.

S. P. Reese · B. J. Ellis · J. A. Weiss
Department of Bioengineering, and Scientific Computing
and Imaging Institute, University of Utah, Salt Lake City, UT, USA

J. A. Weiss
Department of Orthopedics, University of Utah,
Salt Lake City, UT, USA

J. A. Weiss (✉)
Department of Bioengineering, University of Utah, 72 South Central
Campus Drive, Rm. 2750, Salt Lake City, UT 84112, USA
e-mail: jeff.weiss@utah.edu

(Jarvinen et al. 2004; Hurschler et al. 2003). Fibers are arranged in a largely parallel fashion (Kannus 2000). At the mesoscale, fibers are assembled into fascicles (100–500 μm diameter) (Danylchuk et al. 1978; Kannus 2000; Wang 2006). Fascicles are organized in parallel (Haraldsson et al. 2008). At the macroscale, groups of fascicles are organized into functional bands ((100 μm –1 mm) diameter) (Danylchuk et al. 1978).

Force transfer between scales in collagenous soft tissues is poorly understood. At the mesoscopic level, force does not appear to be distributed evenly between fascicles (Haraldsson et al. 2008; Komolafe and Doehring 2010). At the fiber level, the strain is highly inhomogeneous, with the dominant modes of deformation consisting of fiber sliding and uncrimping (Screen et al. 2004a; Screen and Cheng 2007). Tendon failure occurs at both the fiber and fascicle levels (Fung et al. 2009; Nakama et al. 2005; Ritter et al. 2009). Because adjacent fascicles are poorly coupled, this may cause stress shielding of damaged fascicles, adversely affecting the healing response (Haraldsson et al. 2008). Furthermore, vascularization and innervation, which are required for normal function of collagenous soft tissues, occur at the fascicle level. Since mechanotransduction occurs by fibroblasts and tenocytes at the fiber level, abnormal fiber loading (e.g., as a result of fascicle injury or rupture) may adversely affect the fibroblast-mediated remodeling of the tissue (Haraldsson et al. 2008; Wang 2006). At the fibril level, certain disease states (e.g., Ehlers Danlos Syndrome) affect the formation and subsequent strength of collagen fibrils (Tozer and Duprez 2005). Thus, a comprehensive understanding of the mechanical function of normal and diseased connective tissues requires an understanding of multiscale structure–function relationships and the mechanisms of interaction between scale levels.

Although multiscale structure–function relationships are of fundamental importance, the study of these relationships has proved challenging. For instance, studies that have characterized the material properties of different constituents of tendon (e.g., single fascicles, fibers and fibrils) have arrived at conflicting conclusions regarding scale-dependent material behavior (Atkinson et al. 1999; Haraldsson et al. 2008; Hirokawa 2003; Komolafe and Doehring 2010; Miyazaki and Kozaburo 1999; Screen et al. 2004a; Screen and Cheng 2007; Yamamoto et al. 1999). Some studies have found that tissue structures become stiffer with increasing scale (e.g., whole tendon is stiffer than fascicles) (Hirokawa 2003; Miyasaka et al. 1991; Yamamoto et al. 1999), while others have reported the opposite trend (Atkinson et al. 1999; Komolafe and Doehring 2010). These conflicting results may be due to damage of tissue structures during separation, clamping artifacts, errors in measurement of strain and/or cross-sectional area and sample hydration. Further, it is challenging to obtain a homogenous test sample, as the material properties of

tendon and ligament vary between the insertion site and the mid-substance (Thomopoulos et al. 2003; Hewitt et al. 2001; Lake et al. 2009).

The dependence of mechanical behavior on the physical size of the sample is known as a “size effect.” This has been observed in trabecular bone (Park and Lakes 1986; Fatemi et al. 2002) and expanded foams (Anderson and Lakes 1994; Shu et al. 1999). Size effects occur when the size of the microstructure approaches the wavelength of the macroscopic displacement field (Shu et al. 1999). This inadequate separation of characteristic length between the microstructure and macrostructure violates the traditional continuum assumption that microstructures are infinitesimally small relative to the microscale. To model size effects, several higher order theories (e.g., generalized continua, nonlocal elasticity) have been proposed (Anderson and Lakes 1994; Fatemi et al. 2002). In traditional continuum elasticity theory (referred to as the “local continuum assumption” herein), the stress at a point is only a function of the strain at that point. In higher order theories, the stress at a point is a function of both the strain at that point and the surrounding material. Most commonly, this is taken into account via strain gradients (Anderson and Lakes 1994; Fatemi et al. 2002; Kouznetsova et al. 2004). Size effects may occur near constrained boundaries due to large strain gradients or near the cut edges of samples due to a disrupted microstructure. Distinguishing between these two types of size effects is challenging (Anderson and Lakes 1994).

The characteristic size of fascicles ($\sim 200 \mu\text{m}$) and fibers ($\sim 20 \mu\text{m}$) is only 1–3 orders of magnitude smaller than macroscopic tendon dimensions ($\sim 10 \text{mm}$) (Danylchuk et al. 1978; Kannus 2000). Furthermore, the isolation of fibers, fascicles and even whole tendons results in damage that may cause edge effects. Although further experimental verification is needed, size effects within tendon and ligament may lead to the propagation of stress between scales in a manner that is inconsistent with the local continuum assumption (Buechner and Lakes 2003; Kouznetsova et al. 2004).

Unfortunately, the study of size effects in native collagenous connective tissues is wrought with experimental challenges. The preparation of consistent samples, the complicated multiscale organization of these tissues and the difficulty in separating gradient-dependent size effects from edge-dependent size effects complicate the study of multiscale force transfer. This study addressed these challenges by developing a surrogate material and using it as a physical model to isolate and study key structural features. Because of the regular structure of the surrogate, there was no damage along the edges, which allowed for the isolation of gradient-based size effects. Furthermore, the regular structure of the surrogate facilitated the creation of a micromechanical finite element (FE) model, which was validated using a number of strain measures. This allowed certain hypotheses to be

addressed that would be difficult to test using the physical model alone. The objectives of this study were (1) develop a collagen-based physical surrogate and subject it to tensile loading, (2) create a 3D micromechanical FE model of the surrogate and validate it using stress and strain measured at both the macroscale and microscale, (3) examine boundary effects and mesoscale size effects within the surrogate using the validated micromechanical model and a continuum model and (4) perform a sensitivity study to examine the effects of inter-fiber spacing and relative stiffness on predicted strains.

2 Methods

2.1 Surrogate construction

Collagen-based surrogates were created from type I collagen. To create fibers, acid solubilized rat tail tendon collagen (10 mg/ml) was diluted to 5 mg/ml in 1X PBS, neutralized to a pH=8.5, injected into 1-m-long silicone tubes with an inner diameter of 1.4 mm and allowed to polymerize at RT for 8 h. Sulfide-functionalized fluorescent styrene beads ($d = 1.0 \mu\text{m}$, $\lambda_{\text{emission}} = 543 \text{ nm}$, 7.3×10^6 beads/ml) were added to the solution prior to polymerization (Vader et al. 2009). The gel was extruded to form fibers. Fibers were incubated in water overnight and then allowed to dry under their own weight to a final diameter of $\sim 100 \mu\text{m}$ (Caves et al. 2010; Pins et al. 1997).

A custom jig was constructed to align the fibers with a constant spacing. The jig consisted of 1-mm-thick silicone inserts with laser-cut channels ($500 \mu\text{m}$ spacing). These inserts were placed between two glass slides in an acrylic chamber, thus forming a mold. Fibers were placed in the jig, and 5 mg/ml collagen containing carboxyl functionalized fluorescent styrene beads ($1 \mu\text{m}$ diameter, $\lambda_{\text{emission}} = 605 \text{ nm}$, 7.3×10^6 beads/ml) was injected into the chamber and allowed to polymerize overnight. The resulting constructs were cross-linked in a solution of 5% formalin and 2% glutaraldehyde for 8 h. Constructs were then cut to $\sim 2.5 \times 30 \text{ mm}$ and stored in water at 4°C . For SEM imaging, individual fibers and gels (2 mg/ml) were fixed and stained using osmium tetroxide, dehydrated in a graded ethanol series, air dried, sputter coated and imaged using a standard protocol (Iwasaki et al. 2008).

2.2 Surrogate testing

A custom mechanical testing apparatus was created to allow simultaneous measurement of force, macroscopic strain and microscopic strain in the surrogates (Fig. S3). The apparatus was mounted on the stage of an inverted confocal microscope. Surrogates were immersed in a saline bath ($N = 9$) at room temperature, mounted in the clamps and subjected to

incremental stress relaxation testing to determine the quasi-static elastic response (Lujan et al. 2007). A total of six 1% strain increments (6% max strain) were applied at a strain rate of 1%/s, with a relaxation time of 5 min between increments. After equilibration of each strain increment, force was recorded and a confocal z -stack was acquired at the center of the construct at $4\times$ and $10\times$ magnification, using two lasers to excite the red ($\lambda = 543 \text{ nm}$) and green ($\lambda = 488 \text{ nm}$) fluorescent beads. A z -stack of five images with $40 \mu\text{m}$ spacing was acquired at each strain level and magnification.

2.3 Strain measurement

Texture correlation was used to measure strain at the macro- and microscale (Upton et al. 2008; Gilchrist et al. 2007). For each z -stack, the image that was closest to the construct center was used for strain measurement. For macroscale strain measurement, a quadrilateral was defined by four nodes within the $4\times$ image. At each node, a subregion of the image was used as a template. In the next image, acquired at the subsequent strain level, the template images were registered and the nodal displacements were computed. The incremental deformation gradient, $d\mathbf{F}$, was computed from the nodal displacements between each strain level using the FE method of shape function interpolation (Bonet and Wood 1997) (Equation SI 1). The total deformation gradient \mathbf{F}_N for strain level N was computed by multiplying the deformation gradients from all previous strain levels (Equation SI 2), and the infinitesimal strain was computed from the total deformation gradient (Equation SI 3). This yielded the average strain within the quadrilateral.

To obtain the microscale strain, quadrilaterals were defined within the matrix and fiber materials. The strain analysis was identical to that described for the macroscale strain measurement. In general, the measured longitudinal strain was less than the applied clamp strain (e.g., 4–5% optical strain for 6% clamp strain). The longitudinal strain, transverse strain and force were interpolated in time via cubic splines. The average strain across all samples was computed at ten time points up to 4% maximum longitudinal strain. The average Poisson's ratio was computed for each region by performing a linear curve fit to the longitudinal strain $\varepsilon_{\text{long}}$ versus transverse strain $\varepsilon_{\text{trans}}$ data.

2.4 Material characterization of gel and fibers

The material behavior of the extruded fibers and the gel matrix were each represented by a hyperelastic constitutive model consisting of a 3D ellipsoidal fiber distribution (EFD) embedded within an isotropic matrix (Ateshian et al. 2009). Details regarding the constitutive model can be found in the appendix, which is contained within the online supplementary information. Collagen gels and extruded fibers

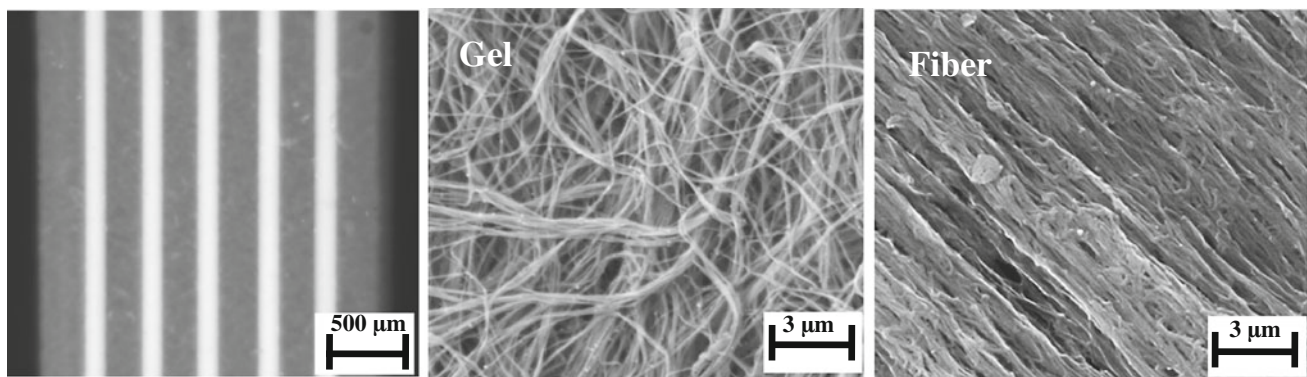


Fig. 1 Structure and organization of the surrogate material. (Left) An overhead photograph of a physical surrogate shows the extruded collagen fibers embedded within the collagen gel. (Middle) SEM imaging

reveals that the gels had loosely and randomly packed collagen fibrils. (Right) In contrast, the fibers had densely packed and highly aligned fibrils

were tested in uniaxial tension using the protocol described previously for the surrogates. For the collagen gel, collagen was polymerized into dog bone-shaped specimens ($N = 12$, gauge length = 20 mm, width = thickness = 2.5 mm, Fig. S3, Panel B) (Roeder et al. 2002). To facilitate clamping, 2-mm-thick sections of melamine foam were polymerized in the specimen ends. For fiber testing, fibers were teased out of assembled, polymerized and fixed surrogates and cut to 40 mm ($N = 15$). As with the surrogate, beads were polymerized in the gel and fibers for strain tracking. Strain was measured using texture correlation. Uniaxial stress–strain data and 2D strain data (ϵ_{long} , ϵ_{trans}) were obtained for both the gels and fibers. A nonlinear constrained pattern search method was used to find the set of coefficients that minimized the sum of the square difference between the data and curve fits for the gel and fiber data sets, with the stress–strain and 2D strain data fit simultaneously (Lewis et al. 2007).

2.5 Micromechanical FE model

A hexahedral FE mesh was constructed to represent the surrogate (Truegrid, XYZ Scientific, Livermore, CA) using the average geometry (Fig. S3, Panel C). The final mesh was chosen based on a mesh convergence study. The EFD model with the best fit coefficients from the gel and fiber testing were used. The surrogate tensile test was simulated by constraining one end of the model in the x – y – z directions and constraining the other end in the x – y plane (the transverse plane). The end constrained in the x – y plane was subjected to displacement boundary conditions in the z -direction that resulted in a clamp-to-clamp strain of 4%. The FEBio finite element software was used for all simulations (<http://www.febio.org>) (Maas et al. 2012). The macroscopic and microscopic strains were calculated from the FE results using the same nodal point coordinates that were used in the experimental texture correlation measurements. This allowed a direct

comparison between the FE and experimental results. To determine the effect of constitutive model parameters, simulations were performed using coefficient values that were ± 1 standard deviation. The best fit coefficient model was compared to the experimental results, and the normalized root mean square error (NRMSE) (Equation SI 14) was used to assess agreement.

3 Results

3.1 Physical surrogate and confocal imaging

Collagen-based physical surrogates ($N = 9$) were constructed by embedding dense, extruded fibers ($\sim 30\%$ by weight) within a collagen hydrogel (0.5% by weight) (Fig. 1, left). The resulting constructs ($l = 30$ mm, $w = 2.42 \pm 0.14$ mm, $t = 1.16 \pm 0.07$ mm) had a mean fiber diameter of 185 ± 20 μm and an inter-fiber spacing of 298 ± 47 μm . SEM imaging revealed that the extruded fibers were composed of densely packed and aligned collagen fibrils (Fig. 1, middle), while the matrix was composed of loosely packed and randomly oriented fibrils (Fig. 1, right). Functionalized styrene beads that were embedded in the gel (red emission) and fiber (green emission) were highly visible at $4\times$ and $10\times$ magnification and proved suitable for use in strain measurement (Fig. 2, left and middle).

3.2 Macroscopic and microscopic strains

Two dimensional strains were measured at the macroscale and the microscale. The macroscopic strain was not representative of the microscopic fiber and matrix strains (Fig. 2, right). At the macroscale, the transverse strain (ϵ_{trans}) induced by the Poisson effect exceeded that of the longitudinally applied strain (ϵ_{long}) and was a nonlinear function of the

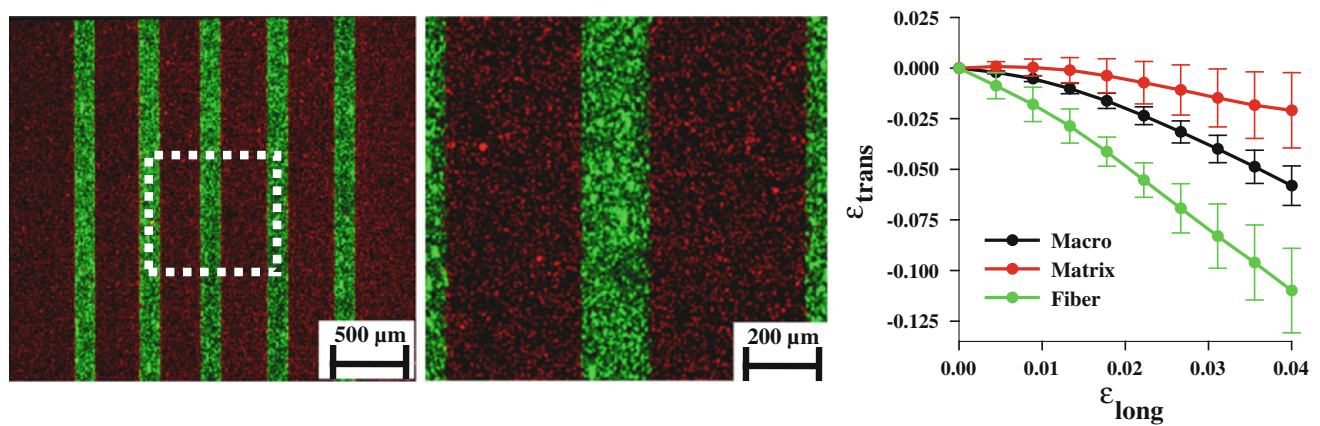


Fig. 2 Confocal images of surrogate constructs and results for microscopic/macroscale strain measurement. (Left) A dual channel 4× image shows the red fluorescent beads in the gel matrix and the green fluorescent beads in the fiber. The dotted white box shows the location of the field for the 10× image that was used for strain analysis. (Middle)

The 10× image from the center of the surrogate used for computing the microscale fiber and gel strain. (Right) The macroscopic transverse strain (black line) was not representative of the microscopic fiber strain (green line) or matrix strain (red line). The error bars represent the standard deviation computed for all samples

longitudinal strain. The average macroscale Poisson's ratio was 1.72 ± 0.26 . The microscale fiber strain in the transverse direction had a magnitude that was considerably larger than the macroscopic value, with an average Poisson's ratio of 2.90 ± 0.56 . Interestingly, the magnitude of the transverse strain for the gel matrix was less than both the fiber and the macroscopic values. The mean matrix Poisson's ratio within the surrogate was 0.57 ± 0.51 . The macroscopically measured stress–strain response was nearly linear, with a modulus of 10.55 ± 1.02 MPa.

3.3 Material characterization of gel and extruded fibers

The constitutive response of the collagen gel and extruded fibers was described using a strain energy-based formulation with an embedded EFD, as discussed in the appendix. The EFD constitutive model was able to simultaneously describe the uniaxial stress–strain and 2D strain behavior of both the extruded fibers ($R^2 = 0.98$) and the collagen gel ($R^2 = 0.99$) (Fig. S1). The fibers were considerably stiffer than the gel ($E_{\text{fiber}} = 215.2 \pm 52.1$ MPa, $E_{\text{gel}} = 0.091 \pm 0.030$ MPa). For both materials, the magnitude of the transverse strain induced by the Poisson's effect exceeded the applied longitudinal strain. The average Poisson's ratios were similar, with the fiber having a Poisson's ratio of 2.86 ± 0.42 and the gel having a Poisson's ratio of 2.84 ± 0.79 . Considerably more variation was seen in the tensile response of the gel than that of the fibers, as indicated by the larger standard deviations for each strain level.

3.4 Micromechanical FE model and validation

The micromechanical FE model was created using the experimentally measured geometry of the surrogate and the curve

fit EFD gel and fiber material coefficients. The model was capable of simultaneously predicting the macroscopic stress–strain behavior as well as the 2D macroscale and microscale strain (Fig. 3). The normalized root mean square error (NRMSE) was used as the metric of comparison between experimental and FE results, as discussed in the appendix. The predicted macroscopic stress (NRMSE=0.015) and the macroscopic transverse strain (NRMSE=0.085) closely matched the experimentally measured values. The predicted microscopic transverse fiber strain was in very good agreement with the experimentally measured values (NRMSE=0.018), while the microscopic transverse matrix strain was not as accurately predicted (NRMSE=0.190). Large variability was present in the experimental results, especially for the macroscopic and matrix 2D strain. When simulations were performed using coefficients that varied from the mean values by a single standard deviation, the predictions closely bounded this uncertainty. This suggests that experimental uncertainty is likely a result of variation of microscale material properties.

3.5 Boundary effects

The influence of the constrained boundary at the clamp interface was examined by varying the aspect ratio of the micro-mechanical FE model from 4:1 to 80:1. Both the microscale matrix transverse strain and the macroscale transverse strain decreased with increasing aspect ratio (Figs. 4, 5). An aspect ratio of 40:1 was needed to reach the values that were obtained for an unconstrained simulation (e.g., no boundary effects). Contour plots of the transverse strain showed that a surrogate model with a constrained boundary had considerable inhomogeneity within the transverse strain field (coefficient of variation = 63.9%) (Fig. 4), while a surrogate model

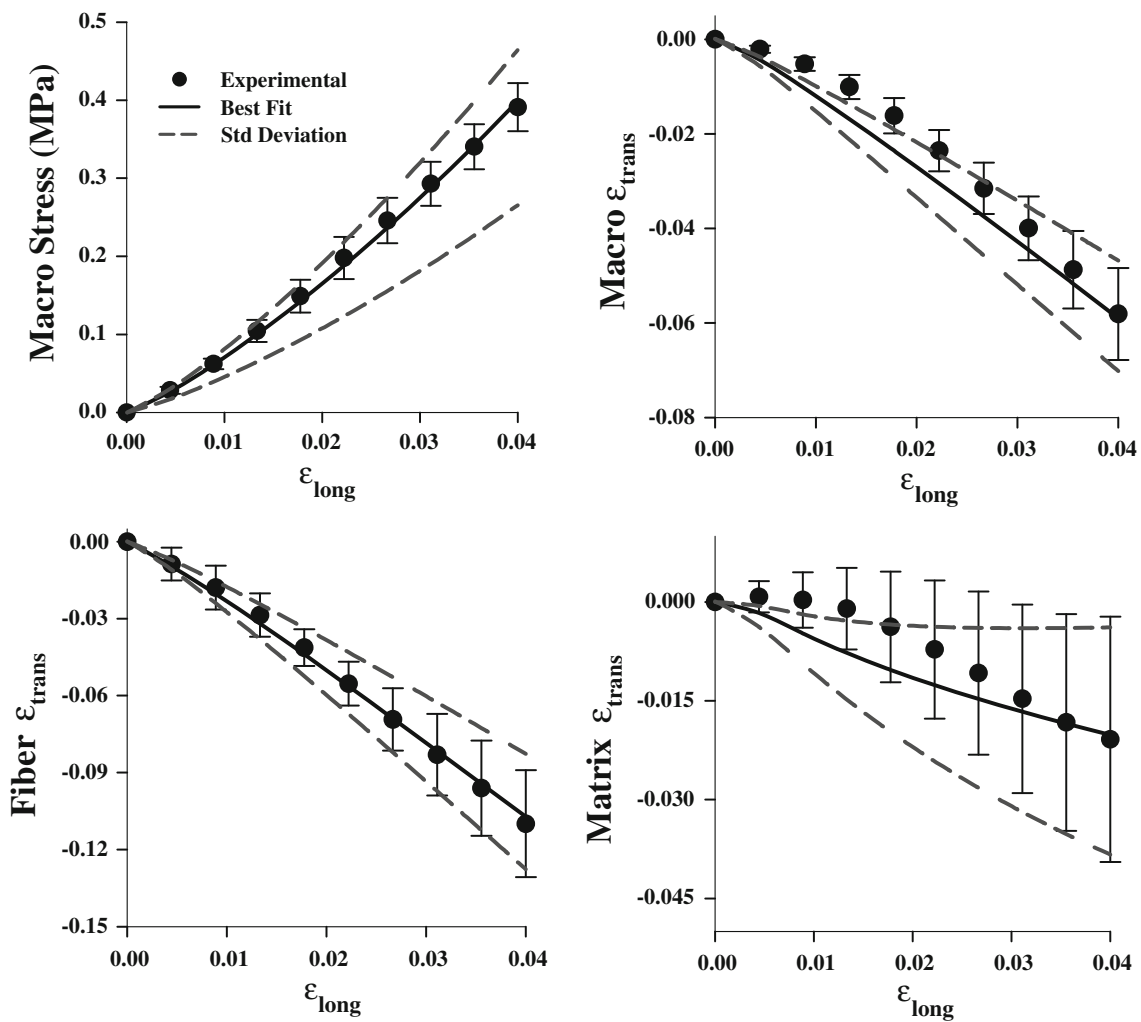


Fig. 3 Micromechanical FE model validation. The FE model predictions were in excellent agreement with the experimental data. Results are shown for the stress–strain (*upper left*), the macroscopic strain (*upper right*), the fiber strain (*lower left*) and the matrix strain (*lower right*).

with an unconstrained boundary did not exhibit this level of inhomogeneity (coefficient of variation = 12.3 %) (Fig. 4). This reveals that the microscale inhomogeneity observed in the mid-substance of the surrogate is generated by a constrained boundary.

3.6 Presence of size effects

To assess the presence of size effects, continuum models with varying aspect ratios were created. Unlike the micromechanical models, which discretely modeled the fibers and the matrix, continuum models featured a homogenized material response applied to the macroscale surrogate dimensions (as discussed in the Appendix). In these simulations, the continuum model only matched the micromechanical model for an aspect ratio of 8:1, which was the aspect ratio for the

surrogate (Fig. 5). Since the material coefficients for the continuum model were obtained by curve fitting the material test data for the surrogate, this result is expected. However, varying the aspect ratio of the continuum model did not result in a significant change in the macroscopic transverse strain, as was observed for the micromechanical model. This indicates that the local continuum assumption is not valid for the surrogate and that size effects are not negligible.

surrogate (Fig. 5). Since the material coefficients for the continuum model were obtained by curve fitting the material test data for the surrogate, this result is expected. However, varying the aspect ratio of the continuum model did not result in a significant change in the macroscopic transverse strain, as was observed for the micromechanical model. This indicates that the local continuum assumption is not valid for the surrogate and that size effects are not negligible.

3.7 Sensitivity studies

Decreasing the inter-fiber distance increased the heterogeneity at the microscale, as indicated by the rise in the microscale strain difference, $\Delta\epsilon_{\text{micro}}$ (Fig. S2). An inter-fiber spacing of $10\ \mu\text{m}$ resulted in a microscale strain difference of $\Delta\epsilon_{\text{micro}} = 0.13$, while the surrogate inter-fiber

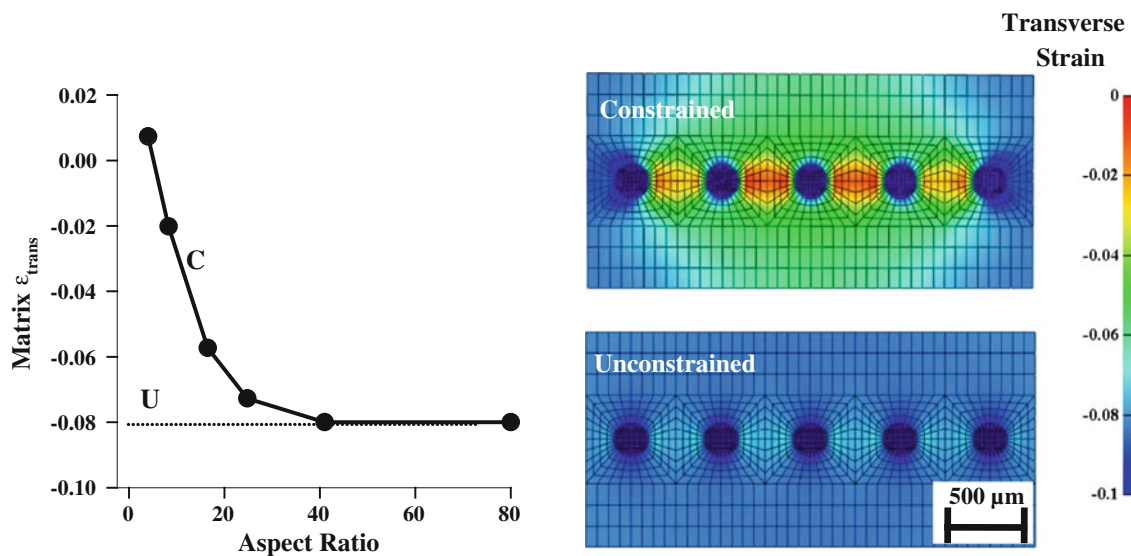


Fig. 4 Effects of aspect ratio and boundary conditions on predictions from micromechanical FE models. (Left) There was a significant reduction in transverse strain with increasing aspect ratio in the surrogate micromechanical FE models. (Middle) The constrained surrogate model displayed considerable heterogeneity in transverse strain, while the

strain field within the unconstrained model was nearly homogeneous. The corresponding point for the constrained model is designated on the plot with a “C”. The dotted line represents the value obtained from the unconstrained model and is labeled with a “U”

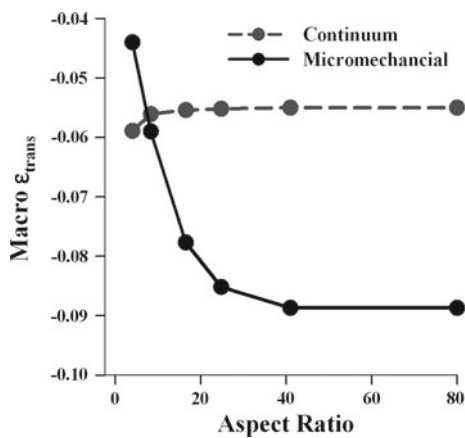


Fig. 5 Effect of aspect ratio on the micromechanical and continuum FE models. Varying the aspect ratio of the micromechanical FE model had a significant impact on the predicted macroscopic transverse strain (solid line), while there was little effect on the continuum FE model (dashed line)

spacing of 300 μm resulted in a microscale strain difference of $\Delta\epsilon_{micro} = 0.08$. Increasing the stiffness of the matrix resulted in a decrease in heterogeneity, as indicated by a lower microscale strain difference with a decrease in the ratio of fiber stiffness to matrix stiffness (E_{fiber}/E_{matrix}) (Fig. S2).

4 Discussion

The physical surrogates created in this study emulated certain structural features found in collagenous soft tissues,

including a nanoscale organization of collagen fibrils and a mesoscale organization of aligned collagen fibers coupled via an inter-fiber matrix. Although the structure of the surrogate was intentionally simplified, the surrogate reproduced a number of experimentally reported observations. The macroscale Poisson’s ratios were in the range of those reported for tendon and ligament (Hewitt et al. 2001; Lynch et al. 2003). At the microscale, the Poisson’s ratio and linear modulus of the extruded fibers matched the experimental values for tendon fascicles (Yin and Elliott 2004), while the modulus of the matrix matched previous estimates for the inter-fiber matrix (Reese et al. 2010; Ault and Hoffman 1992). Poisson’s ratios in excess of the isotropic limit of 0.5 (as reported in this study) are indicative of anisotropy (Reese et al. 2010). In the surrogates, anisotropy was present in both the extruded fibers (via aligned collagen fibrils) and at the macroscale (via aligned extruded fibers). Other anisotropic biological tissues (such as meniscus) also have large estimated Poisson’s ratios (LeRoux and Setton 2002).

The experimentally measured macroscale strain of the physical surrogate was not representative of the microscale strain, which was highly inhomogeneous. The transverse strain within the inter-fiber gel matrix was dissimilar from the transverse strain measured within the fiber. This behavior is qualitatively similar to the inhomogeneous strains experimentally observed at the mesoscale and microscale in tendon tissue (Komolafe and Doehring 2010; Screen et al. 2004a,b).

To investigate the source of this microscale inhomogeneity, a micromechanical model of the physical surrogate was

created. This model was validated at multiple scales and dimensions, which allowed the model to be extended to simulate tests that would have been difficult to perform experimentally. By creating models with varied aspect ratios and comparing them to an unconstrained model, it was revealed that the constrained boundary at the clamp was responsible for the inhomogeneous strain field experimentally observed at the microscale. According to the St. Venant principle in the context of the local continuum theory, the boundary effects should subside (or decay) as the distance from the boundary increases. For highly anisotropic materials, this decay is expected to occur more slowly. In the macroscale continuum model of the surrogate, the boundary effects subsided a short distance from the clamp, thus failing to predict the transmission of the boundary effects into the surrogate mid-substance. In the micromechanical simulations of surrogates with varied lengths, an aspect ratio of nearly 40:1 was needed in order for the boundary effects to subside, as compared to an aspect ratio of 8:1 for an anisotropic continuum model (Figs. 4, 5). This indicates that the local continuum assumption is not valid for describing the macroscale behavior of the surrogate and that size effects are present. Given the large diameter of the fibers relative to the surrogate macroscale dimensions, the presence of these observed size effects is not surprising.

This study did not distinguish between gradient-based size effects and edge-dependent size effects. Because of the regular structure of the surrogate, there was very little damage on the edges. Therefore, we expect that edge-dependent size effects were minimal. It may have been possible to model the two separate types of size effects (e.g., as in Anderson and Lakes 1994) via the inclusion of strain gradients into a continuum-based constitutive model (e.g., Cosserat elasticity or generalized continua). However, such an approach does not allow for the reconstruction of the micro problem (i.e., simulation of the inhomogeneous microscale stress and strain). Multiscale methods were used because of their ability to address both macroscale behavior and microscale behavior.

To determine the relevance of the model in describing the mechanics of native tissue, a sensitivity study was performed. The inter-fiber spacing of the surrogate was much larger than is present in tendon and ligament. Due to manufacturing constraints, the minimum fiber spacing was 300 μm . Smaller spacing resulted in fibers sticking together. Spacing between fascicles within native tendon ranges between 5 and 20 μm . However, the sensitivity study revealed that decreasing the inter-fiber spacing actually led to an increase in the inhomogeneity between the matrix and fiber strain. It has been estimated that the matrix material is 500–5,000 times more compliant than the fibers (Reese and Weiss 2010). A sensitivity study on the matrix stiffness revealed that considerable strain inhomogeneity is present within this range. For a physiologically relevant model with an inter-fiber spacing

of 10 μm and a fiber stiffness $\sim 2,500$ times that of the gel, the predicted matrix strain was positive (matrix $\varepsilon_{\text{trans}} = 0.03$), while the fiber strain was negative (fiber $\varepsilon_{\text{trans}} = -0.10$). If the micromechanical model predictions are indicative of in vivo mesoscale behavior, then these results could have important implications. Histological studies have shown that vessels and nerves are located between fascicles at the mesoscopic level (Kjaer 2004; Wang 2006). If present within native tissue, positive transverse inter-fiber strains may play a role in regulating blood flow. The presence of large negative transverse strains within a fascicle may play a role in nutrient transport. Large strains are indicative of volume loss and thus fluid exudation, as described by biphasic theory (Armstrong et al. 1984; Reese and Weiss 2010; Yin and Elliott 2004).

Since the surrogate represented a simplified physical model, certain features found in native collagenous soft tissues were not reproduced. Fiber crimp was not included, thus the nonlinear stress–strain response typical for tendon was not observed. In this study, cross-linking was performed using formalin and glutaraldehyde, which is not a physiologically occurring mechanism for cross-linking. Finally, other ECM components such as elastin and proteoglycans were not included. Although an attempt to include features such as crimp, alternative cross-linking methods, proteoglycans, etc. may have provided a more physiologically relevant model, it would have come at the cost of simplicity in model construction, analysis and hypothesis testing. Nevertheless, these features can be investigated as part of future studies using the surrogate approach. Although the FE predictions for the stress and 2D strain were quite good, the predicted microscale transverse matrix strain did not fully replicate the experimentally measured behavior. The constructs were observed to shrink a small amount when put into the formalin/glutaraldehyde mixture during their creation. It is hypothesized that the gel shrunk more than the fibers (driven by osmotic forces), which generated a pre-stress within the matrix. Another possible source of error is that of clamping effects on the gel matrix. When testing the gel specimens, it was necessary to embed the tabs in melamine foam. Without this step, the clamping effects affected the tensile response. Since the constructs did not have the foam embedded in the ends that were gripped, this may have introduced an additional clamping effect that was not captured by the FE model. Although the matrix behavior was not perfectly replicated, the predicted result is still within a range deemed acceptable, with a NRMSE of less than 0.2.

The physical surrogate in this study was able to emulate features of the mesoscale microstructure of collagenous soft tissues and allowed for a controlled means of investigating size effects in the presence of a constrained boundary. Sensitivity studies that were performed using the validated micromechanical FE model indicated that the results of this model may have relevance to tissue, where experimental evidence

suggests the presence of such size effects (Komolafe and Doehring 2010; Screen et al. 2004a). In the future, the use of physical models could provide a means for developing and validating more complex and physiologically relevant computational models. Since size effects may play an important role in the normal function of collagenous soft tissues, the results of this work suggest that future modeling studies should carefully consider if a local continuum assumption is adequate for the intended use of the model. In addition to its contribution to the field of multiscale soft tissue mechanics, this study also has relevance to the field of tissue engineering, where computational modeling is poised to help develop future generations of tissue scaffolds.

Acknowledgments Financial support from NIH #R01AR047369, R01EB015133 and R01GM083925 is gratefully acknowledged.

References

- Anderson WB, Lakes RS (1994) Size effects due to Cosserat elasticity and surface damage in closed-cell polymethacrylimide foam. *J Mater Sci* 29:6413–6419
- Armstrong CG, Lai WM, Mow VC (1984) An analysis of the unconfined compression of articular cartilage. *J Biomech Eng* 106(2):165–173
- Ateshian GA, Rajan V, Chahine NO, Canal CE, Hung CT (2009) Modeling the matrix of articular cartilage using a continuous fiber angular distribution predicts many observed phenomena. *J Biomech Eng* 131(6):061003
- Atkinson TS, Ewers BJ, Haut RC (1999) The tensile and stress relaxation responses of human patellar tendon varies with specimen cross-sectional area. *J Biomech* 32(9):907–914
- Ault HK, Hoffman AH (1992) A composite micromechanical model for connective tissues: part II—application to rat tail tendon and joint capsule. *J Biomech Eng* 114(1):142–146
- Birk DE, Zycband EI, Woodruff S, Winkelmann DA, Trelstad RL (1997) Collagen fibrillogenesis in situ: fibril segments become long fibrils as the developing tendon matures. *Dev Dyn* 208(3):291–298
- Bonet J, Wood R (1997) *Nonlinear continuum mechanics for finite element analysis*. Cambridge University Press, Cambridge
- Buechner PM, Lakes RS (2003) Size effects in the elasticity and viscoelasticity of bone. *Biomech Model Mechanobiol* 1(4):295–301. doi:10.1007/s10237-002-0026-8
- Caves JM, Kumar VA, Wen J, Cui W, Martinez A, Apkarian R, Coats JE, Berland K, Chaikof EL (2010) Fibrillogenesis in continuously spun synthetic collagen fiber. *J Biomed Mater Res Part B Appl Biomater* 93(1):24–38. doi:10.1002/jbm.b.31555
- Chang CC, Krishnan L, Nunes SS, Church KH, Edgar LT, Boland ED, Weiss JA, Williams SK, Hoying JB (2011) Determinants of microvascular network topology in implanted neovasculatures. *Arterioscler Thromb Vasc Biol* (in press)
- Danylchuk KD, Finlay JB, Kreck JP (1978) Microstructural organization of human and bovine cruciate ligaments. *Clin Orthop Relat Res* 131:294–298
- Fatemi J, Van Keulen F, Onck PR (2002) Generalized continuum theories: application to stress analysis in bone. *Meccanica* 37:385–396
- Fung DT, Wang VM, Laudier DM, Shine JH, Basta-Pljakic J, Jepsen KJ, Schaffler MB, Flatow EL (2009) Subrupture tendon fatigue damage. *J Orthop Res* 27(2):264–273. doi:10.1002/jor.20722
- Gilchrist CL, Witvoet-Braam SW, Guilak F, Setton LA (2007) Measurement of intracellular strain on deformable substrates with texture correlation. *J Biomech* 40(4):786–794. doi:10.1016/j.jbiomech.2006.03.013
- Haraldsson BT, Aagaard P, Qvortrup K, Bojsen-Moller J, Krogsgaard M, Koskinen S, Kjaer M, Magnusson SP (2008) Lateral force transmission between human tendon fascicles. *Matrix Biol* 27(2):86–95
- Hewitt J, Guilak F, Glisson R, Vail TP (2001) Regional material properties of the human hip joint capsule ligaments. *J Orthop Res* 19(3):359–364
- Hirokawa S (2003) An experimental study of the microstructures and mechanical properties of swine cruciate ligaments. *JSME Int J* 46(4):1417–1425
- Hurschler C, Provenzano PP, Vanderby R Jr (2003) Scanning electron microscopic characterization of healing and normal rat ligament microstructure under slack and loaded conditions. *Connect Tissue Res* 44(2):59–68
- Iwasaki S, Hosaka Y, Iwasaki T, Yamamoto K, Nagayasu A, Ueda H, Kokai Y, Takehana K (2008) The modulation of collagen fibril assembly and its structure by decorin: an electron microscopic study. *Arch Histol Cytol* 71(1):37–44
- Jarvinen T, Jarvinen TL, Kannus P, Jozsa L, Jarvinen M (2004) Collagen fibres of the spontaneously ruptured human tendons display decreased thickness and crimp angle. *J Orthop Res* 22(6):1303–1309
- Kannus P (2000) Structure of the tendon connective tissue. *Scand J Med Sci Sports* 10(6):312–320
- Kjaer M (2004) Role of extracellular matrix in adaptation of tendon and skeletal muscle to mechanical loading. *Physiol Rev* 84(2):649–698. doi:10.1152/physrev.00031.2003
- Komolafe OA, Doehring TC (2010) Fascicle-scale loading and failure behavior of the Achilles tendon. *J Biomech Eng* 132(2):021004. doi:10.1115/1.4000696
- Kouznetsova VG, Geers MGD, Brekelmans WAM (2004) Multi-scale second-order computational homogenization of multi-phase materials: a nested finite element solution strategy. *Comput Methods Appl Mech Eng* 193(48–51):5525–5550. doi:10.1016/j.cma.2003.12.073
- Lake SP, Miller KS, Elliott DM, Soslowsky LJ (2009) Effect of fiber distribution and realignment on the nonlinear and inhomogeneous mechanical properties of human supraspinatus tendon under longitudinal tensile loading. *J Orthop Res* 27(12):1596–1602. doi:10.1002/jor.20938
- LeRoux MA, Setton LA (2002) Experimental and biphasic FEM determinations of the material properties and hydraulic permeability of the meniscus in tension. *J Biomech Eng* 124(3):315–321
- Lewis RM, Shepherd A, Torczon V (2007) Implementing generating set search methods for linearly constrained minimization. *SIAM J Sci Comput* 29(6):2507–2530
- Lujan TJ, Underwood CJ, Henninger HB, Thompson BM, Weiss JA (2007) Effect of dermatan sulfate glycosaminoglycans on the quasi-static material properties of the human medial collateral ligament. *J Orthop Res* 25(7):894–903. doi:10.1002/jor.20351
- Lynch HA, Johannessen W, Wu JP, Jawa A, Elliott DM (2003) Effect of fiber orientation and strain rate on the nonlinear uniaxial tensile material properties of tendon. *J Biomech Eng* 125(5):726–731
- Maas SA, Ellis BJ, Ateshian GA, Weiss JA (2012) FEBio: finite elements for biomechanics. *J Biomech Eng* 134(1):011005–011010
- Miyasaka KC, Daniel DM, Stone ML, Hirshman P (1991) The incidence of knee ligament injuries in the general population. *Am J Knee Surg* 4:3–8
- Miyazaki H, Kozaburo H (1999) Tensile tests of collagen fibers obtained from the rabbit patellar tendon. *Biomed Microdevices* 2(2):151–157
- Nakama LH, King KB, Abrahamsson S, Rempel DM (2005) Evidence of tendon microtears due to cyclical loading in an in vivo tendinopathy model. *J Orthop Res* 23(5):1199–1205. doi:10.1016/j.jorthres.2005.03.006
- Ottani V, Martini D, Franchi M, Ruggeri A, Raspanti M (2002) Hierarchical structures in fibrillar collagens. *Micron* 33(7–8):587–596

- Ottani V, Raspanti M, Ruggeri A (2001) Collagen structure and functional implications. *Micron* 32(3):251–260
- Park HC, Lakes RS (1986) Cosserat micromechanics of human bone: strain redistribution by a hydration sensitive constituent. *J Biomech* 19(5):385–397
- Pins GD, Christiansen DL, Patel R, Silver FH (1997) Self-assembly of collagen fibers. Influence of fibrillar alignment and decorin on mechanical properties. *Biophys J* 73(4):2164–2172
- Reese S, Weiss J (2010) Measurement of Poisson's ratio and transverse strain in rat tail tendon during stress relaxation. In: Proceedings of the 56th annual meeting of the Orthopaedic Research Society, New Orleans, LA, March 5–9 2010
- Reese SP, Maas SA, Weiss JA (2010) Micromechanical models of helical superstructures in ligament and tendon fibers predict large Poisson's ratios. *J Biomech* 43(7):1394–1400. doi:[10.1016/j.jbiomech.2010.01.004](https://doi.org/10.1016/j.jbiomech.2010.01.004)
- Ritter MC, Jesudason R, Majumdar A, Stamenovic D, Buczek-Thomas JA, Stone PJ, Nugent MA, Suki B (2009) A zipper network model of the failure mechanics of extracellular matrices. *Proc Natl Acad Sci U S A* 106(4):1081–1086. doi:[10.1073/pnas.0808414106](https://doi.org/10.1073/pnas.0808414106)
- Roeder BA, Kokini K, Sturgis JE, Robinson JP, Voytik-Harbin SL (2002) Tensile mechanical properties of three-dimensional type I collagen extracellular matrices with varied microstructure. *J Biomech Eng* 124(2):214–222
- Screen HR, Lee DA, Bader DL, Shelton JC (2004a) An investigation into the effects of the hierarchical structure of tendon fascicles on micromechanical properties. *Proc Inst Mech Eng [H]* 218(2):109–119
- Screen HRC, Bader DL, Lee DA, Shelton JC (2004b) Local strain measurement within tendon. *Strain* 40:157–163
- Screen HRC, Cheng VWT (2007) The micro-structural strain response of tendon. *J Mater Sci* 19:8957–8965
- Shu JY, King WE, Fleck NA (1999) Finite elements for materials with strain gradient effects. *Int J Numer Methods Eng* 44(3):373–391. doi:[10.1002/\(sici\)1097-0207\(19990130\)44:3<373:aid-nme508>3.0.co;2-7](https://doi.org/10.1002/(sici)1097-0207(19990130)44:3<373:aid-nme508>3.0.co;2-7)
- Starborg T, Lu Y, Huffman A, Holmes DF, Kadler KE (2009) Electron microscope 3D reconstruction of branched collagen fibrils in vivo. *Scand J Med Sci Sports* 19(4):547–552. doi:[10.1111/j.1600-0838.2009.00907.x](https://doi.org/10.1111/j.1600-0838.2009.00907.x)
- Thomopoulos S, Williams GR, Gimbel JA, Favata M, Soslowky LJ (2003) Variation of biomechanical, structural, and compositional properties along the tendon to bone insertion site. *J Orthop Res* 21(3):413–419
- Tozer S, Duprez D (2005) Tendon and ligament: development, repair and disease. *Birth Defects Res C Embryo Today* 75(3):226–236. doi:[10.1002/bdrc.20049](https://doi.org/10.1002/bdrc.20049)
- Upton ML, Gilchrist CL, Guilak F, Setton LA (2008) Transfer of macroscale tissue strain to microscale cell regions in the deformed meniscus. *Biophys J* 95(4):2116–2124. doi:[10.1529/biophysj.107.126938](https://doi.org/10.1529/biophysj.107.126938)
- Vader D, Kabla A, Weitz D, Mahadevan L (2009) Strain-induced alignment in collagen gels. *PLoS One* 4(6):e5902
- Venturoni M, Gutschmann T, Fantner GE, Kindt JH, Hansma PK (2003) Investigations into the polymorphism of rat tail tendon fibrils using atomic force microscopy. *Biochem Biophys Res Commun* 303(2):508–513
- Vidal DC (2003) Image analysis of tendon helical superstructure using interference and polarized light microscopy. *Micron* 34(8):423–432
- Wang JH (2006) Mechanobiology of tendon. *J Biomech* 39(9):1563–1582. doi:[10.1016/j.jbiomech.2005.05.011](https://doi.org/10.1016/j.jbiomech.2005.05.011)
- Yamamoto E, Hayashi K, Yamamoto N (1999) Mechanical properties of collagen fascicles from the rabbit patellar tendon. *J Biomech Eng* 121(1):124–131
- Yin L, Elliott DM (2004) A biphasic and transversely isotropic mechanical model for tendon: application to mouse tail fascicles in uniaxial tension. *J Biomech* 37(6):907–916